A preliminary study of the influence of ions in the pore solution of hardened cement pastes on the porosity determination by low temperature calorimetry

Min Wu[a,*], Björn Johannesson[a], Mette Geiker[b]

[a]*Department of Civil Engineering, Technical University of Denmark, Building 118, 2800 Lyngby, Denmark*

[b]*Department of Structural Engineering, Norwegian University of Science and Technology, Trondheim, Norway*

Abstract

Thermodynamic modeling was used to predict the ionic concentrations in the pore solution of cement pastes at different temperatures during a freezing and melting measurement in low temperature calorimetry (LTC) studies. By using the predicted ionic concentrations, the temperature depressions caused by the ions presented in the pore solution were determined. The influence of the freezing/melting point depression caused by the ions on the determined pore size distribution by LTC was demonstrated. Thermodynamic modeling using the program PHREEQC were performed on the cylinder and powder samples of cement pastes prepared by two types of cements, i.e., CEM I 32.5 R and CEM III/B 42.5 N. Using the modeled ionic concentrations, the calculated differential pore size distributions for the studied samples with and without considering the temperature depression caused by the ions in the pore solution was compared. The results indicate that for the studied cement paste samples, the influence of the temperature depression caused by the presence of the ions in the pore solution on the determination of the pore size distribution by LTC is limited.

Keywords: Cement paste, low temperature calorimetry, PHREEQC, ionic strength, pore size distribution, thermoporometry, cryoporometry

1. Introduction

Water confined in small pores freeze at lower temperatures compared with that of bulk water. The depressed freezing/melting point of water/ice due to pore confinement is related to the size of the pores [1]. Taking a porous material saturated with water as an example, the water confined in the material will gradually freeze accordingly to the pore sizes (assuming the material has several different pore sizes) as the

*Corresponding author. Tel.: +45 45251813.
Email address: miwu@byg.dtu.dk (Min Wu)

temperature decreases. Similarly, the ice confined in the pores of the material will gradually melt as the temperature increases. As the freezing of water is an exothermic process and the melting of ice is an endothermic process, the heat flow evolution during the freezing and melting process can be recorded by calorimetric devices. Hence, the ice content can be estimated from the recorded heat flow in such a measurement. With the calculated ice content and the thermodynamic relation between pore size and the depressed freezing/melting point combined with other important assumptions, it is possible to determine the pore size distribution for the studied material. This is the principal concept of a method for porosity characterization, i.e., low temperature (micro-)calorimetry or LTC (also known as thermoporometry) [2]. This method was pioneered by researchers in a study of organic gels as early as in the 1950s [3] and later the method was generalized and proposed to be used for different materials, e.g., soil [4] and inorganic materials [5]. In recent years, LTC has experienced further development and it has been used to study many different types of porous materials [6].

The pore system in cement based materials is rather complicated, with the pore sizes ranging from nanometers to millimeters [7, 8]. Porosity is an important parameter for cement based materials, because it influences, e.g., the strength, the shrinkage, the transport properties or permeability and the durability [9] of the materials. Moreover, the characteristics and properties of the pores are important in the modeling and understanding of some important processes for cement based materials, e.g., drying shrinkage [10], carbonation [11, 12] and moisture transport [13, 14]. For these reasons, an accurate characterization of the porosity for cement based materials is of great importance. LTC has been used to study cement based materials, e.g., in [2, 15, 16]. A major advantage of using LTC to characterize cement based materials, compared with the traditional methods developed for porosity characterization, e.g., mercury intrusion porosimetry (MIP), nitrogen adsorption/desorption (NAD) and scanning electron microscopy (SEM), is that the measurements can be conducted on virgin samples without any drying treatment [16–18]. The drying treatment often results in an alteration of the pore structure for cement based materials [19, 20]. It should be mentioned that due to the fact that the liquid present in very small pores does not freeze and that the freezing/melting point depression of liquid in big pores is too small, the pores that can be studied by LTC are limited mainly to those with radii between about 2 nm to about 40 or 50 nm [16, 21]. Water in larger pores is monitored, but the resolution is too limited to allow for determination of the actual pore size. Meanwhile, as an indirect method to study porosity, the analysis of the measured LTC data is not that straightforward. More related discussions can be found, e.g., in [22, 23].

Extensive studies have been conducted with respect to the analysis of LTC data using pure water as the probe liquid, e.g., see [1, 21, 24–26]. However, the analysis of LTC data measured on cement based materials is complicated due to the fact that

the pore liquid is not pure water but contains different types of ionic species [9, 27]. Compared with the freezing/melting of pure water/ice, the presence of ionic species in a pore liquid may mainly cause two effects which would have important impact on the analysis of LTC data. Firstly, the freezing/melting point will be further depressed, depending on the ionic concentration of the pore solution. The temperature depression caused by ions can be predicted if the ionic concentration of the pore solution is known, e.g., see [28, 29]. Secondly, the heat of fusion of the pore solution might be different from that of pure water. It has been demonstrated that the heat of fusion of a pore solution depends on the ionic concentration and the types of ionic species but the exact relation is not clear, e.g., see [30]. That is, even if the ionic concentration and the ionic species of a pore solution are known, the heat of fusion of the pore solution still might not be predictable. The main purpose of this work is trying to study the impact of ions present in cement pore solution on the porosity determination by the LTC method.

One may argue that the impact of ions on the freezing and melting behaviors of the pore solution of cement based materials can be studied by using a model material with a simple pore structure. An artificial cement pore solution can be prepared and used to saturate the model material. By comparing the freezing and melting behaviors of pure water and an artificial pore solution in the same type of model material, the impact of the ions can be studied. However, it should be mentioned that an important characteristic of the pore solution of cement based materials is that the pore walls (cement hydrates) have a great buffering capacity as demonstrated in thermodynamic modeling studies, e.g., see [27, 31, 32], i.e., ions will precipitate when the concentrations in the pore solution are higher than saturation for the considered reactions and ions will diffuse from the cement hydrates into the pore solution if the concentrations are lower than the saturation of the reactions considered. The implication is that the freezing of a pore solution of cement based materials may not be able to be represented or related to the freezing of an artificial cement pore solution in a model material. There is no buffering effect, as described above between pore walls of a model material, e.g., the mostly used silica gels or porous glass, and the artificial pore solution. The artificial cement pore solution in a model material will become more and more concentrated as water freezes out, since the salts are not likely to be included into ice crystals [33, 34]; while the ionic concentration of pore solution of cement based materials might not change that much during freezing depending on the chemical interaction with the cement hydrates. Consequently, the ionic concentration of the artificial pore solution in a model material may differ significantly from the pore solution as more water freezes out in the case of cement based materials, even though the initial concentrations are about the same. Thus, studying the freezing behavior of an artificial cement pore solution in model materials may not necessarily give useful information in the process of understanding the impact of ions on the freezing behavior of the pore solution in

cement based materials.

It is noted that in order to minimize the influence of the ions in the analysis of LTC studies, the preconditioning of cement based samples by curing them in a big amount of (lime)water for a relatively long time has been suggested, e.g., see [15, 16]. In this approach it is assumed that the alkalies leach out of the sample and then allowing the pore liquid to be approximated to be dilute. Consequently the freezing of the diluted pore solution could be assumed as that of pure water [16]. However, a LTC experimental study compared the freezing and melting behaviors of the pore solution of cement paste samples preconditioned in a big amount of saturated limewater for a relatively long time and in a small amount of limewater [35]. The results showed limited difference. That is, it is questionable whether the preconditioning is effective enough. It should also be remarked that the leaching process may result in some changes of the porosity of the studied cement based materials, e.g., see [36, 37].

The difficulty to directly determine the impact of ions in cement pore solution on the freezing and melting behaviors by experiments is realized. Thermodynamic modeling is a very useful tool and it has been applied to cement science very successfully, e.g., see [27, 31, 38–41]. In this work, a preliminary study is conducted to explore the ionic concentrations in the pore solution of cement pastes at different temperatures during freezing and melting measurements in LTC studies. By assuming chemical equilibrium and using experimental LTC data, thermodynamic modeling is used to predict the ionic concentrations in the pore solution of cement pastes. With the predicted ionic concentrations, the temperature depressions caused by the ions can then be determined. The main focus of this work is to demonstrate the influence of the freezing/melting point depression caused by the ions in the pore solution of hardened cement pastes and how this affects the determined pore size distribution.

2. LTC study and results

2.1. Materials and calorimetric measurements

Two types of cement, i.e., CEM I 32.5 R and CEM III/B 42.5 N, were used to prepare the cement paste samples used in this study. The chemical composition of the cements are shown in Table 1. The water-to-cement ratio was 0.4 for all the pastes prepared. The fresh paste samples were mixed by a paddle mixer. After mixing, the fresh pastes were cast into cylindrical plastic vials ensuing proper compaction. The dimension of the plastic vials was about $\phi 15 \times 50$ mm. The hardened cement paste samples were demoulded after one day of sealed curing at room temperature (about 20 °C) and then placed into slightly bigger plastic flasks ($\sim \phi 25 \times 60$ mm) filled with saturated limewater for curing at room temperature. CEM I and CEM III are designated to describe the hardened cement pastes in the following description.

Table 1: Chemical composition of cements (mass%)

Cement	Ig. loss	SiO_2	Al_2O_3	Fe_2O_3	CaO	MgO	SO_3	Na_2O	K_2O
CEM I (32.5R)	2.1	20.6	5.6	2.4	63.4	1.6	2.9	0.2	0.7
CEM III (/B 42.5N)	1.4	29.2	8.9	1.2	48.0	4.8	2.6	0.2	0.6

Both cylinder and powder samples of the cement pastes were studied. To obtain the powder samples, the cylinder samples as prepared were used. The cylinders of cement pastes were firstly vacuum saturated with saturated limewater and then the crushing and grinding of the samples was conducted in a carbon dioxide free chamber to avoid carbonation. After that, the ground paste powders (passed through a 315 μm sieve) were placed into the plastic vials (with dimension of $\phi 15 \times 50$ mm as mentioned earlier, which are used as sample holders) till about half the volume and then saturated limewater was added to immerse the powders. This procedure was also conducted in the carbon dioxide free chamber. In order to saturate the powder samples, the sample holders containing powders covered with saturated limewater were placed under a reduced pressure ($\sim$ 40 mbar) for about 3 hours. After that, the apparent excess bulk water on top of the powders was removed. Then the sample holders with saturated powders were kept standing still for two to three weeks before calorimetric measurements.The cylinder samples used for calorimetric measurements were vacuum saturated first and then the bulk water on the surface of cylinders was wiped off. The total curing time for the cylinder and powder samples were about 1 year and 1.5 years, respectively, before the calorimetric measurements were conducted.

A Calvet-type scanning calorimeter (SETARAM) was used to study the cement pastes. The calorimeter was calibrated and operated to work between about 20 °C and about -130 °C. The cooling and heating rate were set to be 0.1 °C per minute. In the adopted freezing and melting cycle, the temperature scanning started from about 20 °C and went down to about -80 °C and then back to about 20 °C again.

The mass of the tested vacuum saturated samples before calorimetric measurements were measured. After calorimetric measurements, the tested samples were oven-dried at about 105 °C till constant weights. The total water content in each sample was measured by the mass difference between the dry state and the state before the calorimetric measurement. More details about the materials and the measurements can be found in [42].

2.2. Calculated ice content

Based on the measured calorimetric heat flow curves, the ice content in the studied paste samples at different temperatures can be calculated. The results of the calculated

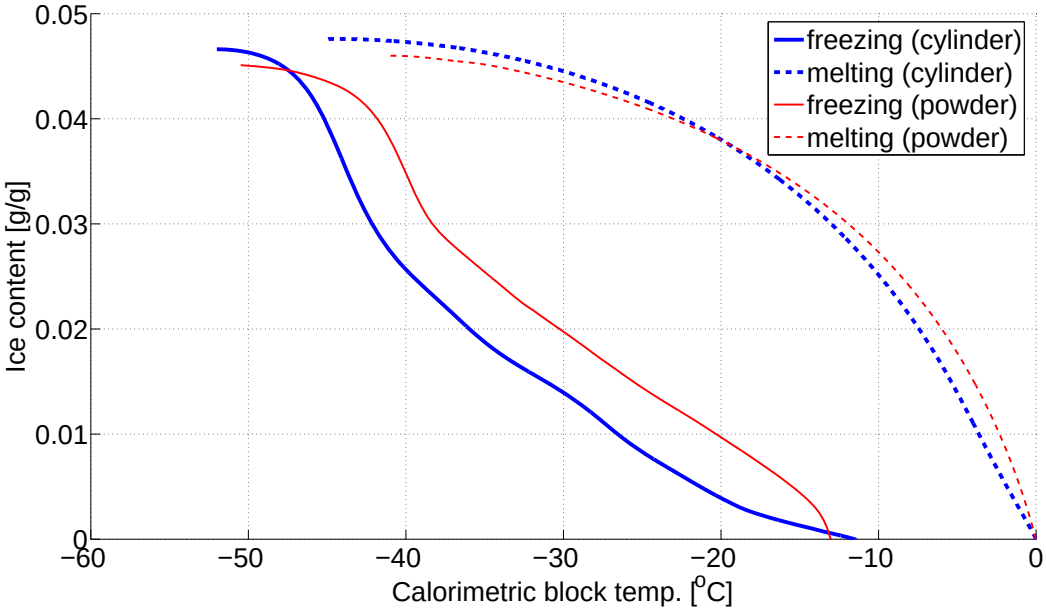

Figure 1: Calculated ice content curves of cylinder and powder samples of the cement paste CEM I (with "bulk" ice subtracted). The content of "bulk" ice in each sample is determined by calculating the ice content corresponding to the peak above 0 °C from the heat flow curve of melting. The ice content is expressed as gram per gram of dry material (g/g). The "bulk" ice determined in the cylinder and the powder sample are about 0.007 and 0.65 g/g, respectively.

ice content for the pastes CEM I and CEM III are presented in Figure 1 and Figure 2, respectively. It should be mentioned that the presented ice content does not include the "bulk" ice, which is determined by calculating the ice content corresponding to the peak above 0 °C from the heat flow curve of melting. For the cylinder samples, the "bulk" ice is mainly the ice in big pores (e.g., air voids) since saturated surface dry samples were used (since the bulk water on the surface of cylinders was wiped off); while for the powder samples, the "bulk" ice should contain both the ice in big air voids and the excess bulk water since there is still a portion of excess water in the powder samples as determined. Detailed discussion concerning the underlying assumptions behind the calculation can be found in [22]. The difference of the calculated ice content between the powder and cylinder samples has been discussed in [42].

As will be described in the next section, the water content in the sample under consideration is an input parameter for predicting the ionic concentration in the pore solution. The calculated ice content curves will be used to determine the remaining water content in the studied samples at different temperatures during LTC measurements. Details will be presented later.

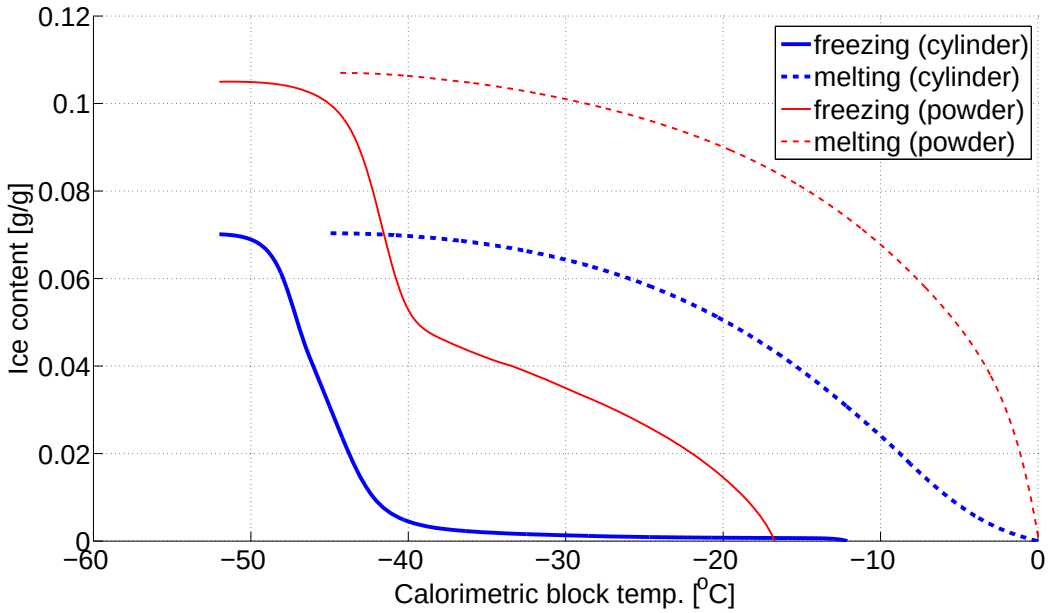

Figure 2: Calculated ice content curves of cylinder and powder samples of the cement paste CEM III (with "bulk" ice subtracted). The content of "bulk" ice in each sample is determined by calculating the ice content corresponding to the peak above 0 °C from the heat flow curve of melting. The ice content is expressed as gram per gram of dry material (g/g). The "bulk" ice determined in the cylinder and the powder sample are about 0.003 and 0.91 g/g, respectively.

3. Modeling the ionic concentration

The freezing of the pore water in cement based materials (due to the relatively wide pore size distribution) typically takes place at a wide range of temperatures. Normally, for ions presented in a certain amount of water, the concentration of the solution would increase as the pore water gradually freezes out [2, 43]. However, the concentration of a cement pore solution may change differently due to the relatively big buffering capacity of cement hydrates as mentioned earlier. The concentrations of different ions in a cement pore solution depend on the equilibrium constants of the involved chemical reactions. The equilibrium constants are normally temperature dependent. It is, therefore, necessary to consider the temperature dependence of the equilibrium constants included in the model to predict he ionic concentration of a cement pore solution. In this work, the thermodynamic phase equilibrium program PHREEQC [44] is used.

In this section, the essential aspects of using the PHREEQC program to predict the ionic concentrations of the pore solution of cement based materials at different temperatures are discussed. It is noted that in the following the hydrated cement minerals are simply referred to as "hydrates" and a chemical reaction is referred to as "dissolution" or "precipitation" depending on the direction of the reaction.

3.1. General description of the PHREEQC program

The PHREEQC program can be used to calculate a solution composition and the solid phase assemblages under equilibrium. This is carried out by solving simultaneously the mass conservation law of master species, law of charge balance and mass-action equations which describe the constitutive relations of aqueous species and hydrates [45].

Equilibrium between the aqueous species and the solid phase assemblages is described by mass-action equations. The mass-action equations can be expressed as

$$K_{a,p} = \prod_i (\gamma_i c_i)^{n_{i,p}} \tag{1}$$

where $K_{a,p}$ is the thermodynamic equilibrium constant of the hydrate p ($p = 1, 2, \cdots, g$; g is the total number of considered hydrates); γ_i and c_i are the activity coefficient and the concentration of ion i, respectively; $n_{i,p}$ is the stoichiometric coefficient of the ion i in hydrate p. The values for $n_{i,p}$ maybe positive or negative. In PHREEQC, terms on the left-hand side of a dissolution reaction are assigned negative coefficients and terms on the right-hand side are assigned positive coefficients.

Activity coefficients of aqueous species are estimated by the Davies equation:

$$\log\gamma_i = -\mathrm{A}z_i^2\left(\frac{\sqrt{\mu}}{1+\sqrt{\mu}} - 0.3\mu\right) \tag{2}$$

or optionally the extended or WATEQ Debye-Hückel equation:

$$\log\gamma_i = -\frac{\mathrm{A}z_i^2\sqrt{\mu}}{1+\mathrm{B}a_i^0\sqrt{\mu}} + b_i\mu \tag{3}$$

where z_i is the ionic charge of aqueous species i; A and B are constants depend only on temperature; μ is the ionic strength of the solution. For Eq.3, it is the extended Debye-Hückel equation if b_i is equal to zero; and it is the WATEQ Debye-Hückel equation if b_i is not equal to zero [46]. In the extended Debye-Hückel equation, a_i^0 is the ion size parameter; while in the WATEQ Debye-Hückel equation, a_i^0 and b_i are ion-specific parameters fitted from mean-salt activity-coefficient data [45]. Unless otherwise specified in the database file or the input data set, the Davies equation is used for charged species in this work.

The thermodynamic database for the aqueous species and the mineral phases used in this study is CEMDATA07 (version 07.02) [47], which is developed with a special focus on cement based systems, e.g., see [27, 39, 40].

It should be noted that more involved constitutive assumptions than that illustrated in Eq. 1 are assumed in describing the equilibrium conditions for some cement hydrates. Due to the mineralogical and chemical complexity of some cement hydrates, an adequate description of all the phases involved in cement hydration is not yet possible. Thus, different assumptions exist for certain types of hydrates, e.g., the C-S-H phase [41, 48, 49] and the AFm phase [27, 38]. More discussions about different chemical models for the solid phases of cement hydrates can be found, e.g., in [50]. For the C-S-H phase, Hydrogarnet phase, Stratlingite phase, Ettringite (AFt) and calcium aluminate monosulfate (AFm) phase, a solid solution method is used in this study. The main precipitation/dissolution reactions considered for cement hydration in this study are listed in Appendix A.

The equilibria of a solid solution phase can be written as in terms of the end members constituting the solid solution, as [45]

$$K_{a,p_{ss}} = \prod_i (\gamma_i c_i)^{n_{i,p_{ss}}} / \lambda_{p_{ss}} x_{p_{ss}} \tag{4}$$

where $K_{a,p_{ss}}$ is the equilibrium (solubility) constant of component p in pure form; $n_{i,p_{ss}}$ is the stoichiometric coefficient of species i in the dissolution reaction for component p in solid solution ss; $x_{p_{ss}}$ is the mole fraction of component p in the solid solution ss; and $\lambda_{p_{ss}}$ is the activity coefficient. The mole fraction of a component in a solid solution is defined as [45]

$$x_{p_{ss}} = n_{p_{ss}} / \sum_{p_{ss}}^{N_{ss}} n_{p_{ss}} \tag{5}$$

where N_{ss} is the number of end members in the solid solution ss. For an ideal solid solution, the activity coefficient $\lambda_{p_{ss}}$ is 1.0.

In short, two types of inputs are essential to calculate the composition of the pore solution of a hardened cement sample using the PHREEQC program, i.e., the initial chemical composition and the solubility constants of involved chemical reactions. The determination of the initial chemical composition of a hardened cement sample and the consideration of the temperature dependent property of solubility constants are presented as follows.

3.2. Chemical composition of a hardened cement sample

The chemical composition of a hardened cement sample involving degree of hydration as an input for the equilibrium calculation using the PHREEQC program can be determined from the characteristic values of cement minerals, i.e., the chemical composition, the hydration degree and the mass concentration.

If there are M kinds of oxides and N kinds of minerals in a cement, the initial chemical composition of a hardened cement to be used in the equilibrium calculation, denoted as a vector $\mathbf{c}$, can be calculated as

$$\begin{aligned} \begin{pmatrix} c_1 \\ \vdots \\ c_M \end{pmatrix} &= \begin{pmatrix} R_{11} & \cdots & R_{1N} \\ \vdots & \ddots & \vdots \\ R_{M1} & \cdots & R_{MN} \end{pmatrix} \begin{pmatrix} \alpha_1 x_1 \\ \vdots \\ \alpha_N x_N \end{pmatrix} \\ &= \begin{pmatrix} R_{11} & \cdots & R_{1N} \\ \vdots & \ddots & \vdots \\ R_{M1} & \cdots & R_{MN} \end{pmatrix} \begin{pmatrix} \alpha_1 & & 0 \\ & \ddots & \\ 0 & & \alpha_N \end{pmatrix} \begin{pmatrix} x_1 \\ \vdots \\ x_N \end{pmatrix} \end{aligned} \tag{6}$$

where c_m $(m = 1, \ldots, M)$ is the content of the mth oxide in a hydrated cement, x_n $(n = 1, \ldots, N)$ is the content of the nth mineral in the cement, α_n is the hydration degree of the nth mineral and R_{mn} is the content of the mth oxide in the nth mineral. The matrix $\mathbf{R}$ (with the elements of R_{mn}) can be determined theoretically from the composition formula of pure minerals (refer to the classical Bogue calculation, e.g., see [51]). When matrix $\mathbf{R}$ is invertible, i.e., $M = N$, the mineral content vector $\mathbf{x}$ consisting of the elements x_n can be calculated by $\mathbf{x} = \mathbf{R}^{-1}\mathbf{p}$, in which $\mathbf{p}$ is the vector containing the mass concentration of the different oxides in the cement. Thus, the input of the initial chemical composition to be used in the equilibrium calculation can be written as

$$\mathbf{c} = \mathbf{R}\text{diag}(\alpha_1, \cdots, \alpha_N)\mathbf{R}^{-1}\mathbf{p} \tag{7}$$

where the diagonal matrix $\text{diag}(\alpha_1, \cdots, \alpha_N)$ includes the hydration degrees of the different minerals, i.e., $\alpha_1, \cdots, \alpha_N$.

3.3. Temperature dependent solubility constant K_a

In PHREEQC, there are two ways to describe the temperature dependent property of the solubility constant K_a for a chemical reaction. If the standard enthalpy of a reaction $\triangle_r H^{\Theta}_{298}$ (at 25 °C) is an input, the temperature dependence of K_a will be considered according to the van't Hoff equation, which is

$$\ln(K_{aT}) \approx \ln(K_{a298}) - \frac{\triangle_r H^{\Theta}_{298}}{R}(\frac{1}{T} - \frac{1}{298}) \tag{8}$$

where K_{aT} is the approximated solubility constant at temperature T (in Kelvin degree) from the solubility constant K_a at temperature 298K (25 °C); R is the gas constant. With the van't Hoff equation and the known solubility constant at one temperature, it is possible to extrapolate the solubility constants at other temperatures. It should be noted that Eq.8 is based on the assumption that the enthalpy of a reaction $\triangle H^{\Theta}_T$ is a constant (i.e., without temperature dependence), which is not necessarily true. Thus, the accuracy of the predicted solubility constants is very much restricted by this assumption. Nevertheless, without further knowledge about the thermodynamic properties at a desired temperature, Eq.8 can provide a rough approximation. The detailed derivation of the temperature dependence of solubility constant K_a and related discussions are presented in Appendix B.

The temperature dependence of K_a can also be defined by an explicit empirical expression in PHREEQC, which is in the form of

$$\log_{10}(K_a) = A_1 + A_2 T + \frac{A_3}{T} + A_4 \log_{10}(T) + \frac{A_5}{T^2} \tag{9}$$

where A_1 to A_5 are five different fitting parameters (constants). If the standard enthalpy and the five constants of the empirical expression are both given as inputs, the empirical expression will be used in preference in the PHREEQC calculation.

The temperature dependence of the solubility constants in terms of the five constants A_1 to A_5 presented in the database CEMDATA07 (version 07.02) [47] is used in this study. No verifications of the validity of the data at freezing temperatures has been made. With no further knowledge about the thermodynamic data, the temperature dependent property of the solubility constants included in the database CEMDATA07 (version 07.02) is used in this work to study the freezing behavior of cement pore solution.

3.4. Input parameters for calculation

To calculate the change of the ionic concentration of a cement pore solution during LTC measurements, the following input parameters are needed:

- Chemical composition of the cement
- Cement content and water content in the sample
- Hydration degree of cement minerals
- Temperature

With the above input parameters, the ionic concentrations of a cement pore solution at different temperatures (with no ice present) can be calculated with the experimentally determined total water content. In order to calculate the ionic concentrations of the pore solution at different temperatures during LTC measurements in the presence of ice, the water content in the studied sample is adjusted by subtracting the corresponding calculated ice content (see Figure 1 and Figure 2) from the total water content.

Parrot and Killoh [52] proposed a set of empirical expressions to predict the hydration degree of cement minerals in OPC, which are

$$R_t = \frac{K_1}{N_1}(1-\alpha_t)(-\ln(1-\alpha_t))^{(1-N_1)} \tag{10}$$

$$R_t = \frac{K_2(1-\alpha_t)^{2/3}}{1-(1-\alpha_t)^{1/3}} \tag{11}$$

$$R_t = K_3(1-\alpha_t)^{N_3} \tag{12}$$

where R_t and α_t are the rate and degree of hydration at time t, respectively; K_1, N_1, K_2, K_3, N_3 are constant parameters and the values for cement minerals are listed in Table 2. Eq.10 is for nucleation and growth; Eq.11 or Eq.12 is for diffusion controlled hydration. The lowest value of R_t is considered as the rate controlling step. The degree of hydration α_t at time t (in days) is then expressed as $\alpha_t = \alpha_{t-1} + \triangle t \cdot R_{t-1}$. Lothenbach and Winnefeld [27] found reasonable agreement between the predicted hydration degrees using the empirical expressions (Eq.10 to Eq.12) together with the parameter values presented in Table 2 and the results based on the XRD semi-quantitative analysis. For the cylinder and powder samples of the cement pastes under consideration, the hydration degree of the minerals are mainly estimated according to the empirical expressions and parameter values proposed by Parrot and Killoh [52] (i.e., Eq.10 to Eq.12 and Table 2). The calculated values are listed in Table 3. It is assumed that the hydration degree of cement minerals in both CEM I and CEM III are the same in this study.

Table 2: Parameters used to calculate the hydration degree of cement (clinker) minerals as a function of time, data from Parrot and Killoh [52].

Parameters	Cement minerals			
	C_3S	C_2S	C_3A	C_4AF
K_1	1.5	0.5	1.0	0.37
N_1	0.7	1.0	0.85	0.7
K_2	0.05	0.006	0.04	0.015
K_3	1.1	0.2	1.0	0.4
N_3	3.3	5.0	3.2	3.7

Table 3: Assumed hydration degree of cement minerals in the samples of cement paste CEM I and CEM III. The age of the the cylinder and power samples are 1 year and 1.5 years, respectively.

Sample	C_3S	C_2S	C_3A	C_4AF	$CaSO_4$[a]
Cylinder	0.95	0.76	1.00	0.89	1.00
Powder	0.96	0.78	1.00	0.91	1.00

[a]The hydration degree is not calculated from the equations proposed by Parrot and Killoh [52] but following the suggestion given in [41].

4. Modeling results

In LTC studies, the ice content curves of melting processes are normally used to calculate the pore interior size distribution, as freezing processes would only indicate the pore entry or neck sizes [16, 21]. Since a main purpose of this study is to demonstrate the influence of ions on the calculated pore (interior) size distribution, the results presented here, therefore, only focus on the melting processes.

The modeled ionic strength for the cement pastes CEM I and CEM III at different temperatures during the melting process are presented in Figure 3. It can be found that for each cement paste (both the cylinder and powder samples), the modeled ionic strength does not change very much during the temperature range between 0 °C and -40 °C. The modeled ionic strength for the pastes CEM I and CEM III are around 0.5 mol/kg water and 0.7 mol/kg water, respectively.

The modeled ionic strength results at different temperatures will be used to calculate the temperature depression caused by the ions. Then the influence of the ions in the pore solution of the studied cement paste samples on the determination of the pore size distribution will be demonstrated by comparing the calculated pore size distribution with and without considering the temperature depression caused by the presence of ions in the pore solution.

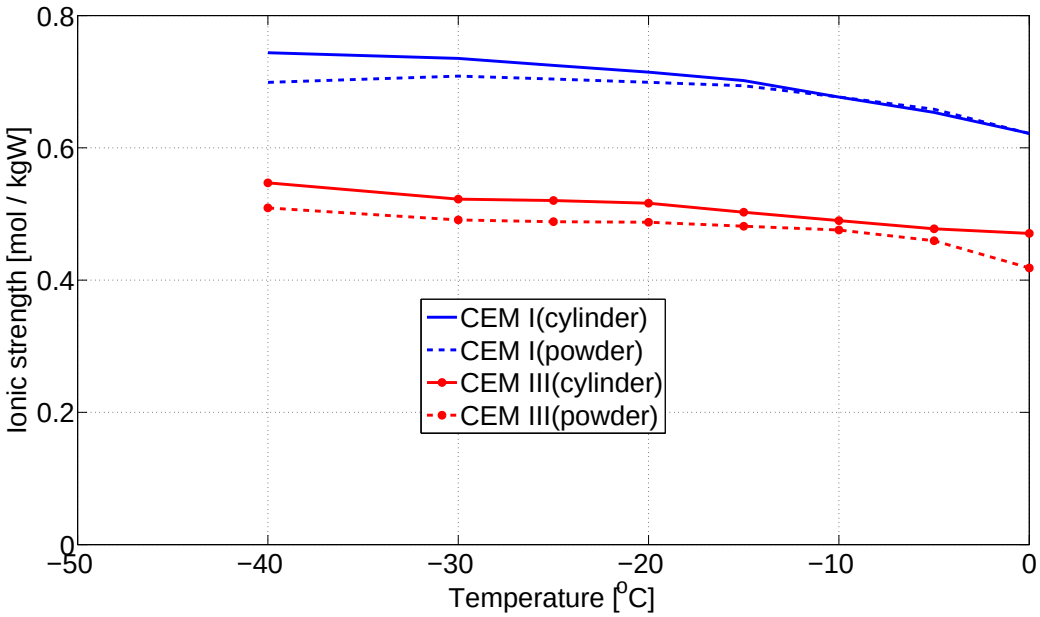

Figure 3: Modeled ionic strength for the cement pastes CEM I and CEM III at different temperatures during the melting process. The ionic strength is expressed as mole per kilogram of water.

5. Influence of the ions on the calculated pore size distribution

5.1. Calculated freezing/melting point depression by the ions

The freezing/melting point depression caused by ions in the pore solution of the cement paste samples can be estimated by using the following equation [28, 29]

$$\triangle T \approx -(\frac{RT_0^2}{\triangle H_A^{fus}})X_B\gamma \tag{13}$$

where $\triangle T$ is the temperature depression, i.e., the difference between the freezing/melting point of the ionic solution and that of pure water T_0; $\triangle H_A^{fus}$ is the heat of fusion of water; X_B is the mole fraction of the solute and γ is the activity coefficient of the solution. For a solution with several types of ions (e.g., cement pore solutions in our case), the activity coefficient γ can be calculated as

$$\gamma = \sum_{i=1}^{N} n_i\gamma_i / \sum_{i=1}^{N} n_i \tag{14}$$

where n_i the mole concentration of the the ith ion in the solution; N is the total number of the ions considered. The detailed derivation of Eq.13 is presented in Appendix C. More discussions about the activity coefficient γ_i and γ can be found, e.g., in [28, 29, 53].

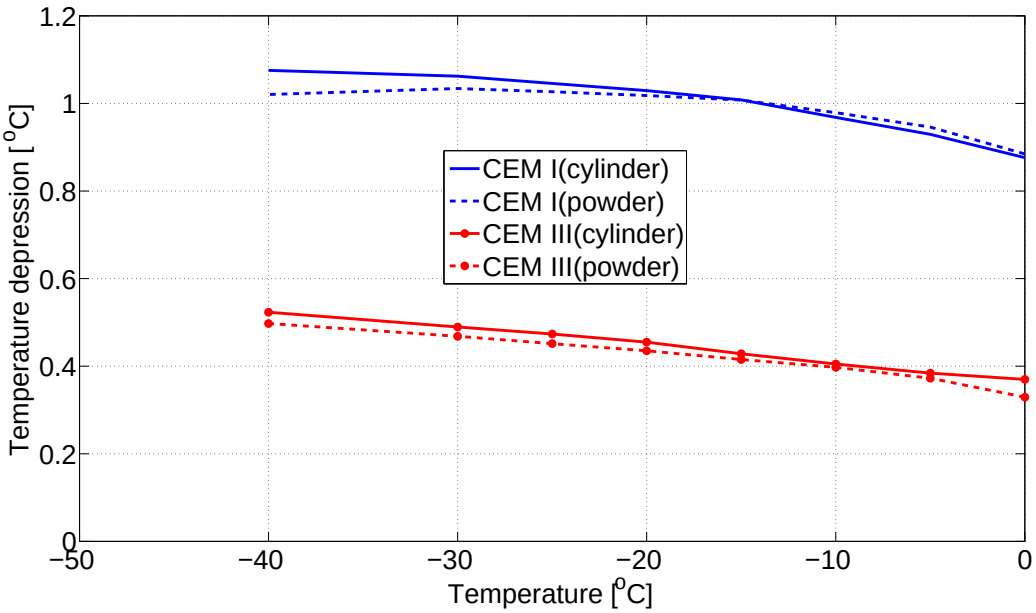

Figure 4: Calculated temperature depression for the cement pastes CEM I and CEM III at different temperatures during the melting process.

The mole concentration n_i and the activity coefficient of each ionic species γ_i are outputs from a PHREEQC calculation. With the obtained n_i and γ_i, the the activity coefficient of a cement pore solution γ can be calculated using Eq.14. The ionic strength μ of a solution in PHREEQC is calculated using [45]

$$\mu = \frac{1}{2}\sum_{i=1}^{N} z_i^2 \frac{n_i}{W_{aq}} \tag{15}$$

where W_{aq} is the mass of the solvent water in the solution. It is noted that the modeled ionic species in a cement pore solution are rather complicated with several different charges. However, to obtain the X_B for a cement pore solution from the modeled ionic strength μ in this study, it is assumed that the ionic charges for the species are ± 1. As can be found from Eq.15, the assumption would result into higher X_B than the true value if the species with charges (absolute value) higher than 1 are important in a solution. That is, the estimated X_B in this study somehow corresponds to the upper limit of the more general case.

With the modeled ionic strength results (presented in Section 4), the temperature depressions caused by the ions in the studied cement paste samples are calculated and shown in Figure 4. The calculated temperature depression for each studied cement paste sample has a relatively small variation during the considered temperature range

(between 0 °C and -40 °C). The variation is about 0.9 °C $\sim$ 1.1 °C for the paste CEM I and about 0.4 °C $\sim$ 0.5 °C for the paste CEM III. The temperature depression caused by the ions will be considered in calculating the pore size distribution.

5.2. Influence of the ions on the calculated pore size distribution

For pure water/ice, the relation between the freezing/melting point depression (or undercooling) caused by the pore confinement and the pore size is assumed to follow the equations proposed by Brun et al. [1], which are

$$R_p = -\frac{32.33}{T - T_0} + 0.68 \tag{16}$$

$$R_p = -\frac{64.67}{T - T_0} + 0.57 \tag{17}$$

where R_p (nm) is the pore size; T is the depressed freezing/melting point of pore water/ice. For melting processes, Eq.16 is used for the cylindrical pore shape assumption and Eq.17 is used for the spherical pore shape assumption. Before further discussion, a clarification is made here about the temperature depression (or undercooling) which is defined as $T - T_0$ in this work.

The relation between the pore radii and the undercooling (in melting) with and without considering the temperature depression caused by the ions in the pore solution of the cylinder samples of the cement pastes CEM I and CEM III are compared in Figure 5. By considering the pore solution as pure water, Eq.16 or Eq.17 is used to calculate the pore radii (according to the assumed pore shape). By considering the pore solution as an ionic solution, the contribution of the temperature depression caused by the ions (Figure 4) to a measured undercooling is excluded when calculating the pore radii using Eq.16 or Eq.17. It can be found that for undercoolings, e.g., higher than about -10 °C, there is some noticeable difference between the calculated pore radii with and without considering the effect caused by the presence of the ions; while for undrcoolings lower than about -10 °C, very limited difference is found between the calculated pore radii. This conclusion also holds for the powder samples, since the temperature depression caused by the ions in the powder and the cylinder samples for each cement paste are almost the same.

The calculated differential pore size distribution considering the pore liquid as pure water or as an ionic solution for the cement pastes CEM I and CEM III are compared in Figure 6 and Figure 7, respectively. There is only some slight difference between the calculated differential pore size distributions for each cement paste sample with and without considering the temperature depression caused by the ions in the pore solution. That is, using the modeled ionic concentrations for the pore solution of the studied cement paste samples, the resulting influence of the temperature depression

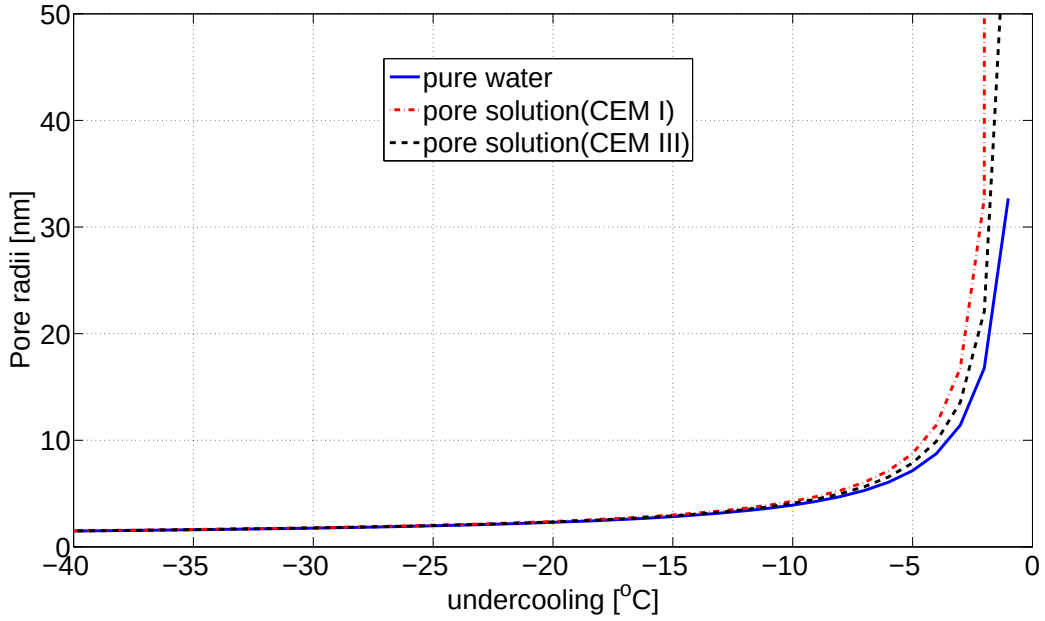

(a)

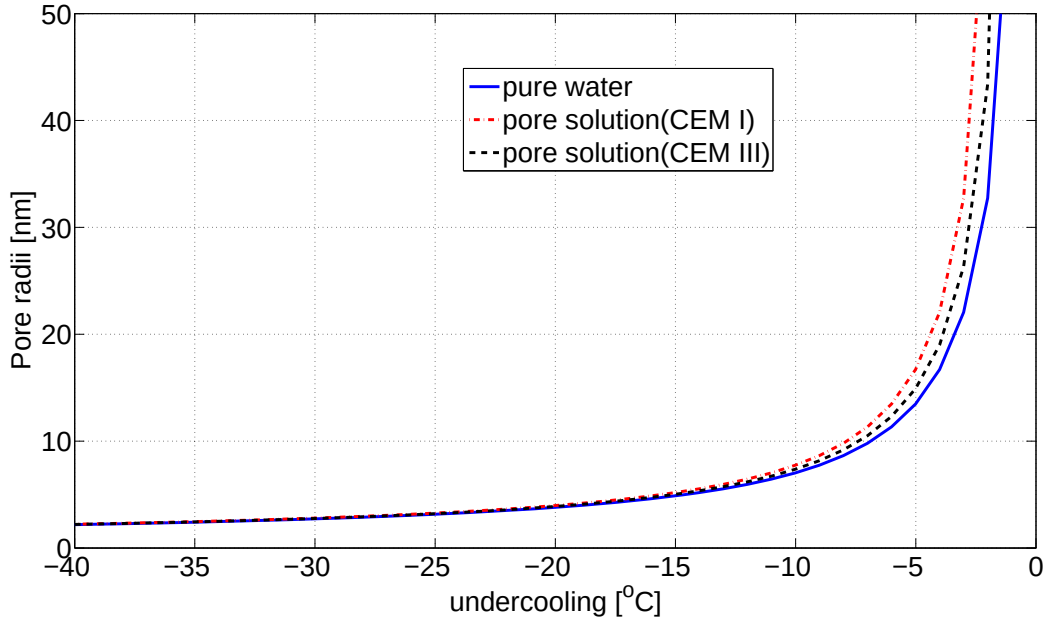

(b)

Figure 5: Comparison of the relation between the pore radii and the undercooling (in melting) with and without considering the temperature depression caused by the ions in the pore solution of the cement pastes CEM I and CEM III (cylinder samples). The pore shape is assumed to be (a) cylindrical and (b) spherical.

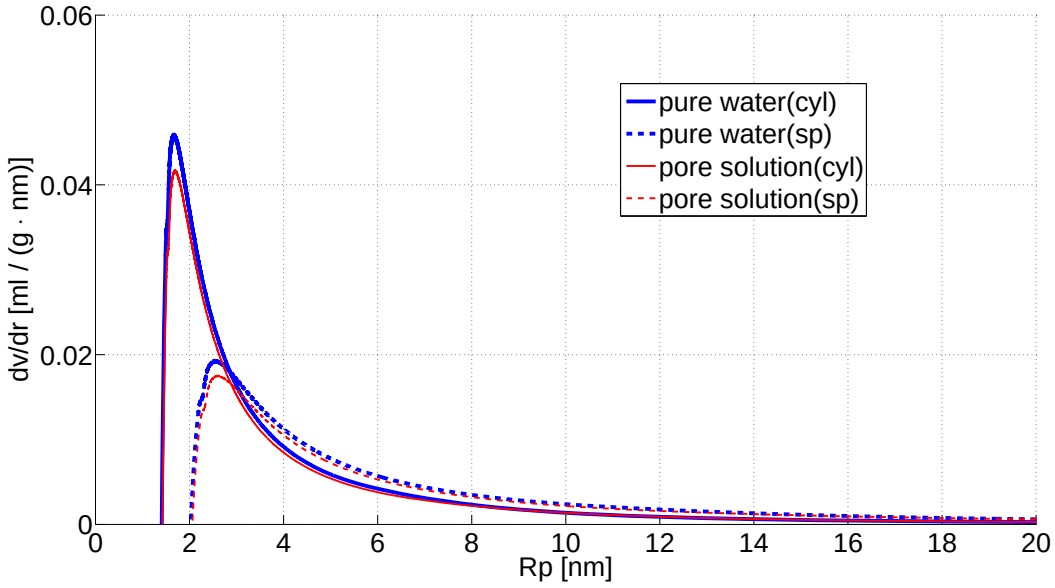

(a)

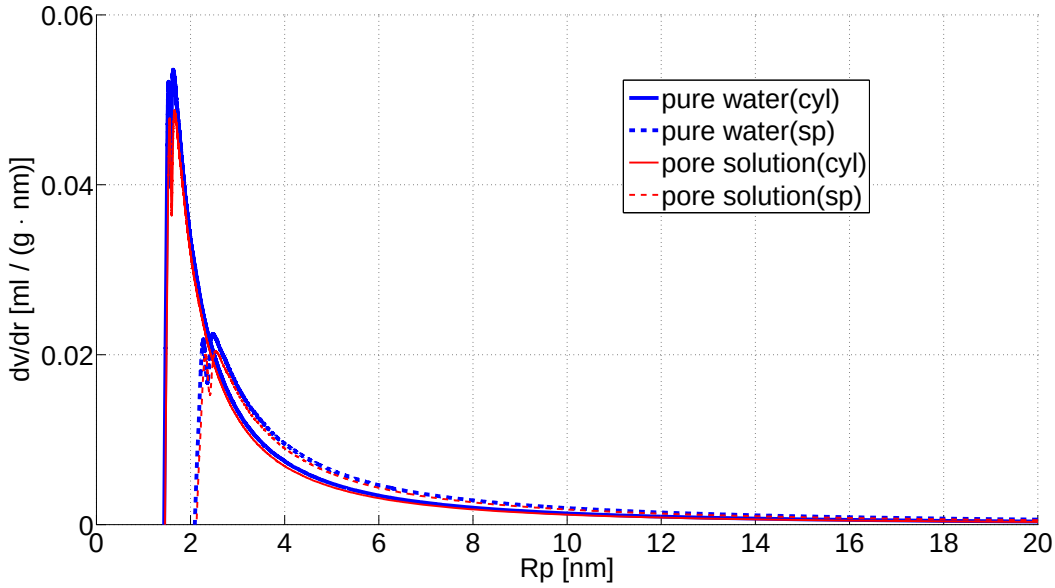

(b)

Figure 6: Calculated differential pore size distribution for the CEM I sample considering the pore liquid as pure water or as an ionic pore solution based on cylindrical (cyl) and spherical (sp) pore assumptions: (a) for the cylinder sample and (b) for the powder sample.

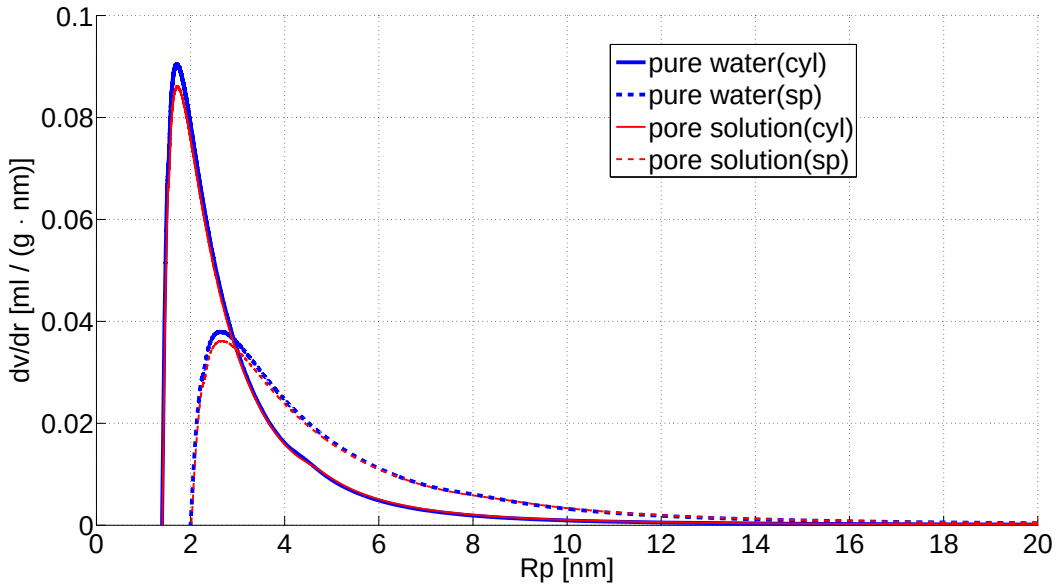

(a)

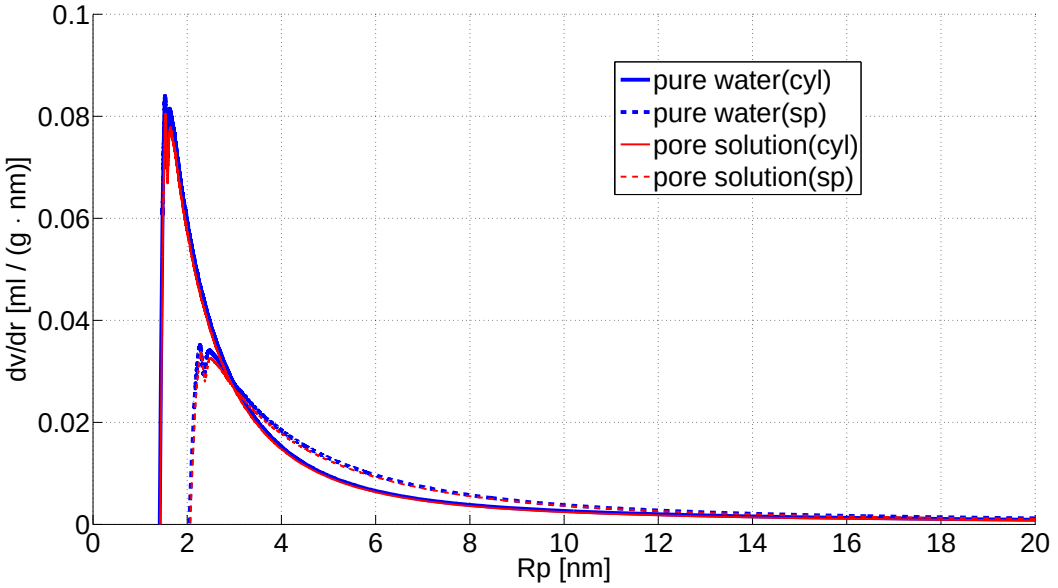

(b)

Figure 7: Calculated differential pore size distribution for the CEM III sample considering the pore liquid as pure water or as an ionic pore solution based on cylindrical (cyl) and spherical (sp) pore assumptions: (a) for the cylinder sample and (b) for the powder sample.

caused by the ions in the pore solution on the pore size distribution determination by LTC is limited.

6. Conclusions

Thermodynamic modeling was used to predict the ionic concentrations in the pore solution of cement pastes at different temperatures during a freezing and melting measurement in LTC studies. That is, it was assumed that the standard thermodynamic relations and concepts can be used also for undercooled water present in the pores of the paste samples. The modeled ionic concentrations were used to determine the temperature depressions caused by the ions presented in the pore solution. The influence of the freezing/melting point depression caused by the ions in the pore solution of hardened cement pastes on the determined pore size distribution by LTC was investigated.

Thermodynamic modeling using the program PHREEQC were performed on the cylinder and powder samples of the cement pastes prepared by two different types of cements. The results showed that the ionic strength for each studied paste sample does not change very much at the temperature range between 0 °C and -40 °C during the LTC measurements. Using the modeled ionic concentrations, the calculated differential pore size distributions for the studied samples with and without considering the temperature depression caused by the ions presented in the pore solution were compared. The results indicate that for the studied cement paste samples in this investigation, the temperature depression caused by the ions present in the pore solution affects the determination of the pore size distribution by LTC to a limited extent.

Acknowledgment

The research leading to these results has received funding from the European Union Seventh Framework Programme (FP7/2007-2013) under grant agreement 264448.

Appendix A: Dissolution/precipitation reactions for cement hydrates

The dissolution/precipitation reactions considered for the cement hydrates in this study are listed in Table 4. The table is mainly based on the chemical models proposed by Kulik [49] and Lothenbach and Winnefeld [27] and it is compiled from a summary prepared by Jensen et al. [50].

Table 4: Dissolution/precipitation reactions for cement hydrates

	Reactions[a]
Pure phases	
Portlandite	$Ca(OH)_2 + 2\,H^+ \leftrightarrow Ca^{2+} + 2\,H_2O$
Brucite	$Mg(OH)_2 + 2\,H^+ \leftrightarrow Mg^{2+} + 2\,H_2O$
Syngenite	$K_2Ca(SO_4)_2H_2O \leftrightarrow Ca^{2+} + 2\,K^+ + 2\,SO_4^{2-} + H_2O$
Gypsum	$CaSO_4{:}2\,H_2O \leftrightarrow Ca^{2+} + SO_4^{2-} + 2H_2O$
Anhydrite	$CaSO_4 \leftrightarrow Ca^{2+} + SO_4^{2-}$
Silica (am)	$SiO_2 + 2\,H_2O \leftrightarrow H_4SiO_4$
$Al(OH)_3$(am)	$Al(OH)_3 + OH^- \leftrightarrow Al(OH)_4^-$
CAH_{10}	$CaAl_2(OH)_8{:}6\,H_2O \leftrightarrow Ca^{2+} + 2\,Al(OH)_4^- + 6\,H_2O$
Solid solutions	
	C-S-H
TobH	$(CaO)_{0.66}(SiO_2)(H_2O)_{1.5} + 1.32H^+ \leftrightarrow 0.66Ca^{2+} + H_4SiO_4 + 0.16H_2O$
TobD	$(CaO)_{0.83}(SiO_2)_{0.66}(H_2O)_{1.83} + 1.66H^+ \leftrightarrow 0.83Ca^{2+} + 0.66H_4SiO_4 + 1.34H_2O$
JenH	$(CaO)_{1.33}(SiO_2)(H_2O)_{2.16} + 2.66H^+ \leftrightarrow 1.33Ca^{2+} + H_4SiO_4 + 1.49H_2O$
JenD	$(CaO)_{1.5}(SiO_2)_{0.66}(H_2O)_{2.5} + 3.00H^+ \leftrightarrow 0.66Ca^{2+} + H_4SiO_4 + 0.16H_2O$
	AFm(1)
C_2AH_8	$Ca_2Al_2(OH)_{10}{:}3\,H_2O \leftrightarrow 2\,Ca^{2+} + 2\,Al(OH)_4^- + 2\,OH^- + 3\,H_2O$
C_2FH_8	$Ca_2Fe_2(OH)_{10}{:}3\,H_2O \leftrightarrow 2\,Ca^{2+} + 2\,Fe(OH)_4^- + 2\,OH^- + 3\,H_2O$
	AFm(2)
C_4AH_{13}	$Ca_4Al_2(OH)_{14}{:}6\,H_2O \leftrightarrow 4\,Ca^{2+} + 2\,Al(OH)_4^- + 6\,OH^- + 6\,H_2O$
C_4FH_{13}	$Ca_4Fe_2(OH)_{14}{:}6\,H_2O \leftrightarrow 4\,Ca^{2+} + 2\,Fe(OH)_4^- + 6\,OH^- + 6\,H_2O$
	AFm(3)
C_2ASH_8	$(CaO)_2Al_2O_3SiO_2{:}8\,H_2O \leftrightarrow 2\,Ca^{2+} + 2\,Al(OH)_4^- + H_3SiO_4^- + OH^- + 2\,H_2O$
C_2FSH_8	$(CaO)_2Fe_2O_3SiO_2{:}8\,H_2O \leftrightarrow 2\,Ca^{2+} + 2\,Fe(OH)_4^- + H_3SiO_4^- + OH^- + 2\,H_2O$
	AFm(4)
$C_4A\bar{S}H_{12}$	$(CaO)_3Al_2O_3(CaSO_4){:}12\,H_2O \leftrightarrow 4\,Ca^{2+} + 2\,Al(OH)_4^- + SO_4^{2-} + 4\,OH^- + 6\,H_2O$
$C_4F\bar{S}H_{12}$	$(CaO)_3Fe_2O_3(CaSO_4){:}12\,H_2O \leftrightarrow 4\,Ca^{2+} + 2\,Fe(OH)_4^- + SO_4^{2-} + 4\,OH^- + 6\,H_2O$
	Hydrogarnet
C_3AH_6	$(CaO)_3Al_2O_3{:}6\,H_2O \leftrightarrow 3\,Ca^{2+} + 2\,Al(OH)_4^- + 4\,OH^-$
C_3FH_6	$(CaO)_3Fe_2O_3{:}6\,H_2O \leftrightarrow 3\,Ca^{2+} + 2\,Fe(OH)_4^- + 4\,OH^-$
	AFt
Al-Ettringite	$Ca_6Al_2(SO_4)_3(OH)_{12}{:}26\,H_2O \leftrightarrow 6\,Ca^{2+} + 2\,Al(OH)_4^- + 3\,SO_4^{2-} + 4\,OH^- + 26\,H_2O$
Fe-Ettringite	$Ca_6Fe_2(SO_4)_3(OH)_{12}{:}26\,H_2O \leftrightarrow 6\,Ca^{2+} + 2\,Fe(OH)_4^- + 3\,SO_4^{2-} + 4\,OH^- + 26\,H_2O$
	Strätlingite
Al-Strätlingite	$Ca_2Al_2SiO_2(OH)_{10}{:}3\,H_2O \leftrightarrow 2\,Ca^{2+} + 2\,Al(OH)_4^- + SiO(OH)_3^- + OH^- + 2\,H_2O$
Fe-Strätlingite	$Ca_2Fe_2SiO_2(OH)_{10}{:}3\,H_2O \leftrightarrow 2\,Ca^{2+} + 2\,Fe(OH)_4^- + SiO(OH)_3^- + OH^- + 2\,H_2O$

[a]Reactions involving carbon dioxide is not included in the calculation considering the samples were always cured under saturated limewater.

Appendix B: Temperature dependence of solubility constant K_a

The chemical equilibrium of a reaction is defined by the Gibbs free energy. Each component participated in a chemical reaction has its own Gibbs free energy relative to a fixed reference, which can be expressed as

$$G_i = G_i^{\Theta} + RT\ln(a_i) \tag{18}$$

where a_i is the activity ($a_i = \gamma_i c_i$), G_i is the molar Gibbs free energy for component i and G_i^{Θ} is the standard reference value. Due to the minimization of the total Gibbs free energy of a reaction at equilibrium, the change of the standard reference values of the Gibbs free energy of a chemical reaction, $\triangle_r G_T^{\Theta}$, can be expressed as [54]

$$\triangle_r G_T^{\Theta} = -RT\ln(K_a) \tag{19}$$

According to the relation between Gibbs free energy, enthalpy and entropy, i.e., $G = H - TS$, the same relation also holds for the properties with the standard reference values, which can be written as

$$\triangle_r G_T^{\Theta} = \triangle_r H_T^{\Theta} - T\triangle_r S_T^{\Theta} \tag{20}$$

This relation can be regarded as the relation between the Gibbs free energy, enthalpy and entropy for a specific chemical reaction. The entropy property is not always that straightforwardly measurable. However, through mathematical derivations, it is possible to replace the entropy with some other property which can be measured more easily. Under constant pressure, the definition of entropy is $S = -(dG/dT)_P$. In a similar reasoning as used to obtain Eq.20, one can obtain

$$\triangle_r S_T^{\Theta} = -\frac{d(\triangle_r G_T^{\Theta})}{dT} \tag{21}$$

By inserting Eq.21 into Eq.20, one obtains

$$\frac{d(\triangle_r G_T^{\Theta})}{dT} = \frac{\triangle_r G_T^{\Theta} - \triangle_r H_T^{\Theta}}{T} \tag{22}$$

By using a mathematical manipulation, the Gibbs-Helmholtz equation can be obtained, that is

$$\begin{aligned}\frac{d}{dT}(\frac{\triangle_r G_T^{\Theta}}{T})_P &= \triangle_r G_T^{\Theta}\left(\frac{d}{dT}(\frac{1}{T})\right)_P + \frac{1}{T}\left(\frac{d(\triangle_r G_T^{\Theta})}{dT}\right)_P \\ &= -\frac{\triangle_r G_T^{\Theta}}{T^2} + \frac{1}{T}\left(\frac{d(\triangle_r G_T^{\Theta})}{dT}\right)_P = \frac{1}{T}\left(\left(\frac{d(\triangle_r G_T^{\Theta})}{dT}\right)_P - \frac{\triangle_r G_T^{\Theta}}{T}\right)\end{aligned} \tag{23}$$

Combining Eq.23 and Eq.22, the Gibbs-Helmholtz equation is obtained, as

$$\frac{d}{dT}(\frac{\triangle_r G_T^\Theta}{T})_P = -\frac{\triangle_r H_T^\Theta}{T^2} \tag{24}$$

Then, assuming $\triangle_r G_T^\Theta$ and K_a to be temperature dependent functions and applying differentiation on both side of Eq.19 followed by rearrangement gives

$$\frac{d\ln(K_a)}{dT} = -\frac{1}{R}\frac{d}{dT}(\frac{\triangle_r G_T^\Theta}{T}) \tag{25}$$

Combining Eq.24 and Eq.25, the result is

$$\frac{d\ln(K_a)}{dT} = -\frac{\triangle_r H_T^\Theta}{RT^2} \tag{26}$$

For a system under constant pressure, the change of enthalpy $\triangle H$ against temperature T is related by the change of heat capacity $\triangle Cp^\Theta$, which is $(d(\triangle H)/dT)_P = \triangle Cp$. Thus, for a chemical reaction, the change of enthalpy (the standard reference value) $\triangle_r H_T^\Theta$ at temperature T can be expressed as

$$\triangle_r H_T^\Theta = \triangle_r H_{T_0}^\Theta + \int_{T_0}^{T} \triangle_r C_p dT \tag{27}$$

where $\triangle_r H_{T_0}^\Theta$ is the change of enthalpy of the chemical reaction at the temperature T_0, which is normally a constant reference with a known value.

By assuming different temperature dependencies of the heat capacity, C_p, the dependence of the solubility constant K_a on the temperature can be obtained as follows.

1. Assuming $C_p = a_1 + a_2T + a_3T^{-2} + a_4\sqrt{T} + a_5T^2$ ($a_1, a_2, \ldots, a_5$ are fitting parameters) and inserting it into Eq.27, an analytical expression of $\triangle_r H_T^\Theta$ is obtained. Inserting the obtained analytical expression of $\triangle_r H_T^\Theta$ into Eq.26 followed by integration, K_a is obtained and it can be expressed as [55, 56]

$$\log_{10}(K_a) = A_1' + A_2'T + \frac{A_3'}{T} + A_4'\ln(T) + \frac{A_5'}{T^2} + A_6'T^2 + A_7'\sqrt{T} \tag{28}$$

where $A_1', A_2', \ldots, A_7'$ are constants. If the entropy (S^Θ), the enthalpy (H^Θ) and the coefficients of the heat capacity equation ($a_1, a_2, \ldots, a_5$) for the components in reaction are known, the constants $A_1', A_2', \ldots, A_7'$ can be directly calculated [57, 58]. Otherwise, the constants can be obtained by fitting available experimental data to Eq.28. It should be mentioned that the analytical expression for the temperature dependence of K_a adopted in PHREEQC (Eq.9) is based on five

terms, which is slightly different from the expression including seven terms as derived above. The difference is due to that the heat capacity C_p is assumed to be represented with three fitting parameters as, $C_p = a'_1 + a'_2 T + a'_3 T^{-2}$, in the approach adopted in PHREEQC.

2. Assuming the heat capacity of the chemical reaction $\triangle_r C_p$ is a constant in the considered temperature range, the temperature dependence of K_a can be reduced to an approximation including three fitting parameters as [38]

$$\log_{10}(K_a) = A'_1 + \frac{A'_3}{T} + A'_4 \ln(T) \tag{29}$$

3. Assuming the heat capacity of the chemical reaction $\triangle_r C_p = 0$, i.e., the enthalpy $\triangle_r H_T^{\ominus}$ in the considered temperature range is a constant, the temperature dependence of K_a can be expressed as

$$\log_{10}(K_a) = A'_1 + \frac{A'_3}{T} \tag{30}$$

It is noted that Eq.30 is of the same format as the van't Hoff equation described before, i.e., Eq.8.

More discussions about the extrapolation of the temperature dependent solubility constant K_a can be found, e.g., in [55, 56]. Using the extrapolated temperature dependence of solubility constants to study cement based materials can be found, e.g., in [27, 31, 38, 39, 58–60]

Appendix C: Freezing/melting point depression by ions

The thermodynamic basics describing the freezing point depression caused by ions are discussed in this section. The thermodynamic background for this kind of problem can be found in general physical chemistry books, e.g., in [28, 29].

Under equilibrium condition, the relation between infinitesimal change of the temperature, the pressure and the chemical potential of the solvent (pure water in our case) in a pore solution can be expressed by Gibbs-Duhem equations [61], which is

$$S_A^l dT - V_A^l dP_A^l + n_A^l d\mu_A^l = 0 \tag{31}$$

where S is the entropy, T is the temperature in Kelvin degree, V, P, μ, n are the volume, pressure, chemical potential and moles of the solvent A in liquid phase l, respectively. Assuming constant temperature, i.e., $dT = 0$, Eq.31 reduces to

$$n_A^l d\mu_A^l = V_A^l dP_A^l \tag{32}$$

By further assuming that the ideal gas law applies, which means

$$V_A^l = \frac{n_A^l RT}{P_A^l} \tag{33}$$

where R is the gas constant. Inserting Eq.33 into Eq.32 and differentiating yields

$$\int_{\mu=\mu_A^{l^0}}^{\mu=\mu_A^l} d\mu_A^l = \int_{P=P_A^{l^0}}^{P=P_A^l} \frac{RT}{P_A^l} dP_A^l; \qquad \mu_A^l = \mu_A^{l^0} + RT\ln(\frac{P_A^l}{P_A^{l^0}}) \tag{34}$$

where $\mu_A^{l^0}$ is the reference chemical potential of the pure water and $P_A^{l^0}$ is its corresponding reference pressure.

The effect of the composition of a solution on its chemical potential can be assessed by introducing Rault's law which states that the partial pressure of a component is proportional to its mole fraction in the solution, i.e.,

$$X_A = \frac{P_A^l}{P_A^{l^0}} \tag{35}$$

where X_A is the mole fraction of the solvent A in the solution. Taking Rault's law into consideration, the difference between the chemical potential of pure water and the water containing ions can according to Eq.34 be expressed as

$$\mu_A^l = \mu_A^{l^0} + RT\ln(X_A) \tag{36}$$

At the temperature when the water freezes, the three phases of the water, i.e., liquid (l), solid (s) and gas (g), are under equilibrium, indicating their chemical potentials are equal. That is, $\mu_A^l = \mu_A^s$, where μ_A^s is the chemical potential of solid ice. It should be noted that the ice crystals formed in a pore solution are no different from that formed from pure water, since the ions will be expelled out and will not be included into the crystalline structure of ice during freezing, e.g., see [33]. By introducing $X_B = 1 - X_A$, where X_B is the mole fraction of the dissolved solutes in the solution, and replacing μ_A^l with μ_A^s in Eq.36, one obtains

$$\ln(1 - X_B) = \frac{\mu_A^s - \mu_A^{l^0}}{RT} \tag{37}$$

According to classical thermodynamics, the difference between the chemical potentials μ_A^s and $\mu_A^{l^0}$ can be regarded as the molar Gibbs free energy, that is

$$\mu_A^s - \mu_A^{l^0} = \triangle G_A^{l-s} = \triangle G_A^{fus} \tag{38}$$

Similarly, the difference between the entropies (S) and the enthalpies (H) of the liquid and the solid phase is denoted as

$$S_A^s - S_A^{l^0} = \triangle S_A^{fus}; \qquad H_A^s - H_A^{l^0} = \triangle H_A^{fus} \tag{39}$$

Since $G = H - TS$, Eq.38 and Eq.39 can be combined to obtain

$$\triangle G_A^{fus} = \triangle H_A^{fus} - T\triangle S_A^{fus} \tag{40}$$

Further inserting Eq.40 into Eq.37, it gives

$$\ln(1 - X_B) = \frac{\triangle H_A^{fus}}{RT} - \frac{\triangle S_A^{fus}}{R} \tag{41}$$

Considering $X_B = 0$, i.e., the case of pure water, Eq.41 becomes

$$\frac{\triangle H_A^{fus}}{RT_0} - \frac{\triangle S_A^{fus}}{R} = 0 \tag{42}$$

where T_0 is the freezing point of pure water. Inserting Eq.42 into Eq.41, the relation between the freezing point of the water containing ions with a mole fraction of X_B (T) and that of the pure water (T_0) can be established as

$$\ln(1 - X_B) = \frac{\triangle H_A^{fus}}{R}(\frac{1}{T} - \frac{1}{T_0}) \tag{43}$$

Further simplification of Eq.43 can be made by assuming that the the solution is weak, i.e., $X_B \ll 1$, and that the depressed freezing point is not significantly different from that of the pure water, i.e., $T \approx T_0$. That is to say,

$$\ln(1 - X_B) \approx -X_B; \qquad \frac{1}{T} - \frac{1}{T_0} = \frac{T - T_0}{TT_0} \approx \frac{\triangle T}{T_0^2} \tag{44}$$

where $\triangle T = T - T_0$, i.e., the freezing point depression. Thus, Eq.43 can be approximated as

$$X_B \approx -\frac{\triangle H_A^{fus}\triangle T}{RT_0^2} \tag{45}$$

Rearrangement of Eq.45 gives

$$\triangle T \approx -(\frac{RT_0^2}{\triangle H_A^{fus}})X_B \tag{46}$$

It is noted that the prediction by Eq.46 has been confirmed by experimental results for solutions with relatively low concentrations [28]. The derivation of Eq.46 is based on an ideal solution. When the concentrations of a solution is high, the solution could be far from ideal and the freezing point depression could differ greatly from what is

predicted by Eq.46, e.g., as pointed out in [53]. Normally, the activity coefficient γ is introduced in order to account for non-ideal solutions. The equation used is

$$\triangle T \approx -(\frac{RT_0^2}{\triangle H_A^{fus}})X_B\gamma \tag{47}$$

More discussions about the validity of the proposed equations and the determination of the involved parameters can be found, e.g., in [28, 29, 53].

Reference

[1] M. Brun, A. Lallemand, J. Quinson, C. Eyraud, A new method for the simultaneous determination of the size and shape of pores: the thermoporometry, Thermochimica Acta 21 (1) (1977) 59–88.

[2] A. Kjeldsen, M. Geiker, On the interpretation of low temperature calorimetry data, Materials and Structures 41 (1) (2008) 213–224.

[3] W. Kuhn, E. Peterli, H. Majer, Freezing point depression of gels produced by high polymer network, Journal of Polymer Science 16 (82) (1955) 539–548.

[4] P. Williams, Properties and behavior of freezing soils, Tech. Rep. 72, Norwegian Geotechnical Institute, Oslo,Norway (1961).

[5] J. Blachere, J. Young, The freezing point of water in porous glass, Journal of the American Ceramic Society 55 (6) (1972) 306–308.

[6] J. Riikonen, J. Salonen, V. Lehto, Utilising thermoporometry to obtain new insights into nanostructured materials (review part 1), Journal of Thermal Analysis and Calorimetry 105 (2011) 811–821.

[7] A. Neville, Properties of concrete, 4th Edition, Prentice Hall, 1995.

[8] S. Diamond, Aspects of concrete porosity revisited, Cement and Concrete Research 29 (8) (1999) 1181–1188.

[9] H. Taylor, Cement chemistry, 2nd Edition, Thomas Telford, London, 1997.

[10] V. Baroghel-Bouny, M. Mainguy, T. Lassabatere, O. Coussy, Characterization and identification of equilibrium and transfer moisture properties for ordinary and high-performance cementitious materials, Cement and Concrete Research 29 (8) (1999) 1225–1238.

[11] M. Thiery, V. Baroghel-Bouny, G. Villain, P. Dangla, Numerical modeling of concrete carbonation based on durability indicators, in: V. Malhotra (Ed.), Proceedings of the 7th CANMET/ACI International Conference on Durability of Concrete, 2006, pp. 765–780.

[12] B. Bary, A. Sellier, Coupled moisture–carbon dioxide–calcium transfer model for carbonation of concrete, Cement and Concrete Research 34 (10) (2004) 1859–1872.

[13] V. Baroghel-Bouny, Water vapour sorption experiments on hardened cementitious materials. Part II: Essential tool for assessment of transport properties and for durability prediction, Cement and Concrete Research 37 (3) (2007) 438–454.

[14] V. Baroghel-Bouny, M. Mainguy, O. Coussy, Isothermal drying process in weakly permeable cementitious materials- assessment of water permeability, in: International Conference on Ion and Mass Transport in Cement-Based Materials, 1999, pp. 59–80.

[15] G. Fagerlund, Determination of pore-size distribution from freezing-point depression, Materials and Structures 6 (3) (1973) 215–225.

[16] Z. Sun, G. Scherer, Pore size and shape in mortar by thermoporometry, Cement and Concrete Research 40 (5) (2010) 740–751.

[17] R. F. Feldman, The porosity and pore structure of hydrated portland cement paste, in: J. S. L.R. Roberts (Ed.), Pore Structure and Permeability of Cement based Materials, Vol. 137, Materials Research Society, Pittsburgh, PA, 1989, pp. 59–73.

[18] J. Thomas, H. Jennings, A. Allen, The surface area of hardened cement paste as measured by various techniques, Concr. Sci. Eng 1 (1999) 45–64.

[19] J. Villadsen, Pore structure in cement based materials, Tech. Rep. 277, Building Materials Laboratory, Technical University, Denmark (1992).

[20] R. Espinosa, L. Franke, Influence of the age and drying process on pore structure and sorption isotherms of hardened cement paste, Cement and Concrete Research 36 (10) (2006) 1969–1984.

[21] M. Landry, Thermoporometry by differential scanning calorimetry: experimental considerations and applications, Thermochimica Acta 433 (1-2) (2005) 27–50.

[22] M. Wu, B. Johannesson, M. Geiker, Determination of ice content in hardened concrete by low temperature calorimetry: influence of baseline calculation and heat of fusion of confined water, Journal of Thermal Analysis and Calorimetry 115 (2) (2014) 1335–1351.

[23] M. Wu, B. Johannesson, Impact of sample saturation on the detected porosity of hardened concrete using low temperature calorimetry, Thermochimica Acta 580 (2014) 66–78.

[24] K. Ishikiriyama, M. Todoki, K. Motomura, Pore size distribution (PSD) measurements of silica gels by means of differential scanning calorimetry I. optimization for determination of PSD, Journal of Colloid and Interface Science 171 (1) (1995) 92–102.

[25] K. Ishikiriyama, M. Todoki, Pore size distribution measurements of silica gels by means of differential scanning calorimetry II. thermoporosimetry, Journal of Colloid and Interface Science 171 (1) (1995) 103–111.

[26] K. Morishige, K. Kawano, Freezing and melting of water in a single cylindrical pore: The pore-size dependence of freezing and melting behavior, The Journal of Chemical Physics 110 (1999) 4867.

[27] B. Lothenbach, F. Winnefeld, Thermodynamic modelling of the hydration of portland cement, Cement and Concrete Research 36 (2) (2006) 209–226.

[28] P. Atkins, J. De Paula, Physical Chemistry, 8th Edition, Oxford University Press, 2006.

[29] K. Laidler, J. Meiser, Physical Chemistry, 3rd Edition, Houghton Mifflin Company, Boston, 1999.

[30] G. Mrevlishvili, P. Privalov, Calorimetric study of the melting of frozen aqueous solutions of electrolytes, Journal of Structural Chemistry 9 (1) (1968) 5–7.

[31] B. Lothenbach, Thermodynamic equilibrium calculations in cementitious systems, Materials and Structures 43 (10) (2010) 1413–1433.

[32] S. Setunge, N. Nguyen, B. Alexander, L. Dutton, Leaching of alkali from concrete in contact with waterways, Water, Air, & Soil Pollution: Focus 9 (5-6) (2009) 381–391.

[33] G. Scherer, Freezing gels, Journal of non-crystalline solids 155 (1) (1993) 1–25.

[34] J. Kaufmann, Experimental identification of ice formation in small concrete pores, Cement and Concrete Research 34 (8) (2004) 1421–1427.

[35] M. Wu, K. Fridh, B. Johannesson, M. Geiker, Influence of frost damage and sample preconditioning on the porosity characterization of cement based materials using low temperature calorimetry, Microporous and Mesoporous Materials, Submitted for publication (2014).

[36] K. Haga, S. Sutou, M. Hironaga, S. Tanaka, S. Nagasaki, Effects of porosity on leaching of ca from hardened ordinary portland cement paste, Cement and Concrete Research 35 (9) (2005) 1764–1775. doi:http://dx.doi.org/10.1016/j.cemconres.2004.06.034.

[37] M. Mainguy, C. Tognazzi, J. Torrenti, F. Adenot, Modelling of leaching in pure cement paste and mortar, Cement and Concrete Research 30 (1) (2000) 83–90.

[38] D. Damidot, B. Lothenbach, D. Herfort, F. Glasser, Thermodynamics and cement science, Cement and Concrete Research 41 (7) (2011) 679–695.

[39] B. Lothenbach, T. Matschei, G. Möschner, F. Glasser, Thermodynamic modelling of the effect of temperature on the hydration and porosity of portland cement, Cement and Concrete Research 38 (1) (2008) 1–18.

[40] T. Schmidt, B. Lothenbach, M. Romer, K. Scrivener, D. Rentsch, R. Figi, A thermodynamic and experimental study of the conditions of thaumasite formation, Cement and Concrete Research 38 (3) (2008) 337–349.

[41] Y. Hosokawa, K. Yamada, B. Johannesson, L. Nilsson, Development of a multi-species mass transport model for concrete with account to thermodynamic phase equilibriums, Materials and Structures 44 (9) (2011) 1577–1592.

[42] M. Wu, K. Fridh, B. Johannesson, M. Geiker, Impact of sample crushing on the porosity characterization of hardened cement pastes by low temperature calorimetry: comparison of powder and cylinder samples, Journal of Thermal Analysis and Calorimetry, Submitted for publication (2014).

[43] Z. Sun, G. Scherer, Effect of air voids on salt scaling and internal freezing, Cement and Concrete Research 40 (2) (2010) 260–270.

[44] P. Parker, A. Collins, Dehydration of flocs by freezing, Environmental Science & Technology 33 (3) (1999) 482–488.

[45] D. L. Parkhurst, C. Appelo, User's guide to PHREEQC (Version 2): A computer program for speciation, batch-reaction, one-dimensional transport, and inverse geochemical calculations, US Geological Survey Denver, 1999.

[46] A. Truesdell, B. Jones, WATEQ, a computer program for calculating chemical equilibria of natural waters, Journal of Research of the U.S. Geological Survey 2 (1974) 233–274.

[47] EMPA Database, Thermodynamic data for hydrated solids in portland cement system, accessed on March 25, 2013.
URL http://www.empa.ch/plugin/template/empa/*/62204

[48] A. Nonat, The structure and stoichiometry of C-S-H, Cement and Concrete Research 34 (9) (2004) 1521–1528.

[49] D. Kulik, Improving the structural consistency of C-S-H solid solution thermodynamic models, Cement and Concrete Research 41 (5) (2011) 477–495.

[50] M. M. Jensen, B. Johannesson, M. R. Geiker, Framework for reactive mass transport: Phase change modeling of concrete by a coupled mass transport and chemical equilibrium model, Computational Materials Science, Submitted for publication (2014).

[51] B. Johannesson, Cement clinker composition and phases 3B, lecture notes for Introduction to Concrete Technology (11563), Technical University of Denmark (2011).

[52] L. Parrot, D. Killoh, Prediction of cement hydration, in: Proc. Br. Ceram. Soc., no. 35, 1984, pp. 41–53.

[53] B. Johannesson, Classical thermodynamics and its use in understanding freezing and thawing of concrete 12A(A), lecture notes for Introduction to Concrete Technology (11563), Technical University of Denmark (2011).

[54] B. Johannesson, Chemical equilibrium of cement-based materials 5A(B), lecture notes for Introduction to Concrete Technology (11563), Technical University of Denmark (2011).

[55] G. Anderson, D. Crerar, Thermodynamics in geochemistry: The equilibrium model, Vol. 588, Oxford University Press New York, 1993.

[56] J. Munoz, D. Nordstrom, Geochemical Thermodynamics, 2nd Edition, Blackwell, Boston, 1994.

[57] J. Ederová, V. Šatava, Heat capacities of C_3AH_6, C_4ASH_{12} and $C_6AS_3H_{32}$, Thermochimica Acta 31 (1) (1979) 126–128.

[58] D. Damidot, F. Glasser, Thermodynamic investigation of the CaO-Al_2O_3-$CaSO_4$-H_2O system at 50 °C and 85 °C, Cement and Concrete Research 22 (6) (1992) 1179–1191.

[59] D. Kulik, Minimising uncertainty induced by temperature extrapolations of thermodynamic data: a pragmatic view on the integration of thermodynamic databases into geochemical computer codes, in: The use of thermodynamic databases in performance assessment, OECD, Barcelona, 2002, pp. 125–137.

[60] T. Matschei, B. Lothenbach, F. Glasser, Thermodynamic properties of Portland cement hydrates in the system CaO-Al_2O_3-SiO_2-$CaSO_4$-$CaCO_3$-H_2O, Cement and Concrete Research 37 (10) (2007) 1379–1410.

[61] R. Defay, I. Prigogine, A. Bellemans, D. Everett, Surface tension and adsorption, Longmans London, 1966.